PNAS
www.pnas.org

Supplementary Material for

Multiscale imaging of basal cell dynamics in the functionally-mature mammary gland

This PDF file includes:

www.pnas.org/cgi/doi/10.1073/pnas.2016905117

Figure S1

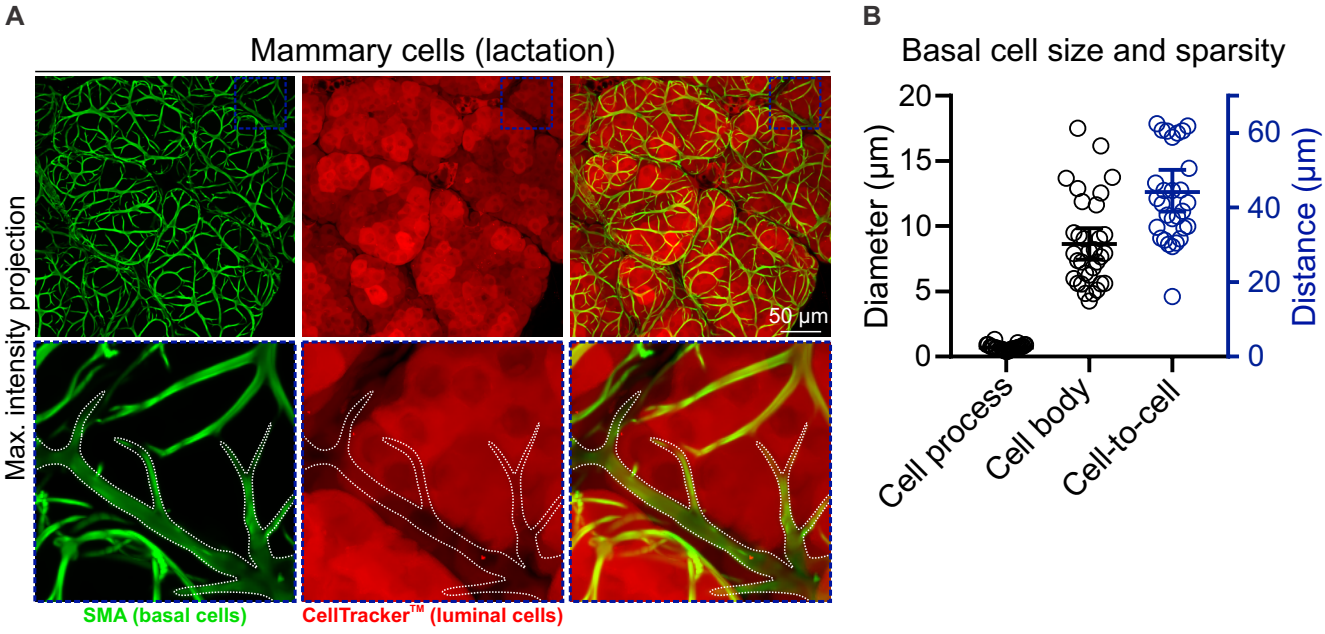
A
Mammary cells (lactation)
Max. intensity projection
50 µm
SMA (basal cells)
CellTracker™ (luminal cells)
B
Basal cell size and sparsity
Diameter (µm)
Distance (µm)
20
15
10
5
0
60
40
20
0
Cell process
Cell body
Cell-to-cell

Fig. S1.

Morphology and density of mammary alveolar basal cells. (**A**) Maximum intensity *z*-projection (0-22 μm) of lactating mammary tissue immunostained with smooth muscle actin (SMA, green) to reveal the cellular morphology and distribution of alveolar basal cells. Tissue was stained with CellTracker™ prior to fixation to show luminal cell layer (red). Dotted line outlines part of a single basal cell. (**B**) Basal cell diameter at the thinnest cell process and at the cell body (left y-axis). Graph also shows the distance between the body of each basal cell and its closest basal neighbor (right y-axis). Basal cells are separated from their closest neighbor by a distance that is approximately 6× their maximum width. Spatial resolution = 0.3 μm; 33 cells analyzed from n = 3 mice.

Figure S2

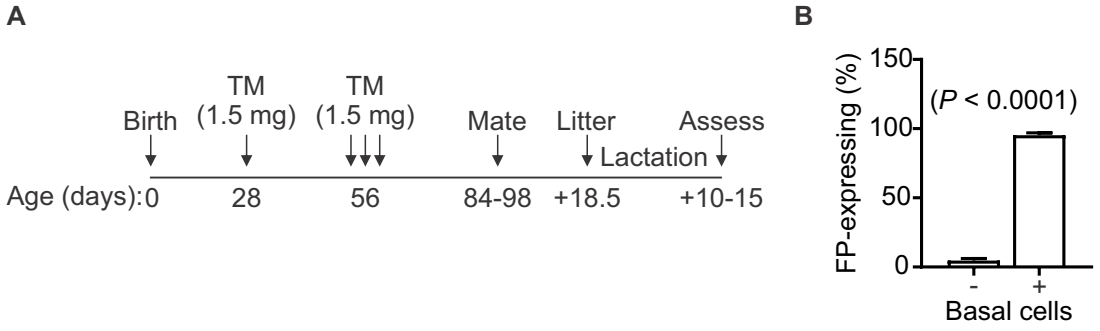
A
Birth
TM
(1.5 mg)
TM
(1.5 mg)
Mate
Litter
Assess
Lactation
Age (days):0
28
56
84-98
+18.5
+10-15
B
FP-expressing (%)
150
100
50
0
(P < 0.0001)
-
+
Basal cells

Fig. S2.

Induction and analysis of fluorescent protein (FP) expression in basal cells. (**A**) Schematic representation of the mouse model and experimental timeline (see also Methods). (**B**) The percentage of SMA-positive basal cells that express the FP. Positivity was scored from 3D image sequences of cleared tissue; 2400 cells counted from n = 3 mice. $P < 0.0001$, Student's t-test. No FP-positive luminal cells were identified in any of the image sequences. TM, tamoxifen.

Figure S3

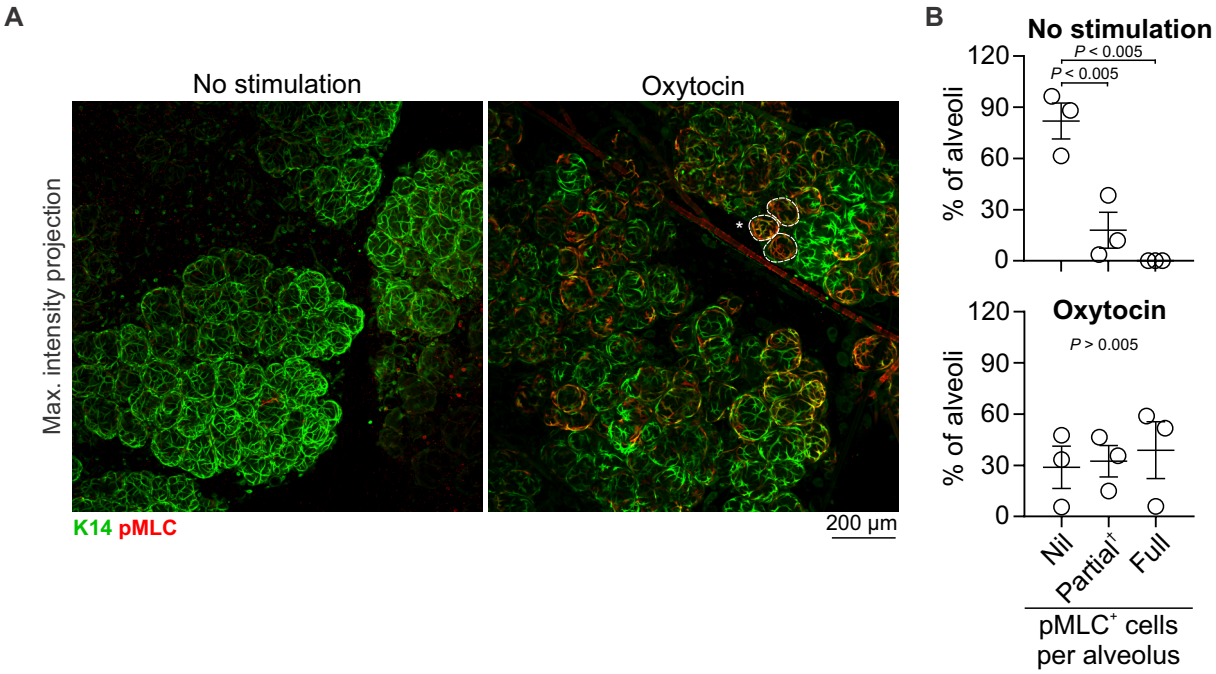
A
No stimulation
Oxytocin
Max. intensity projection
K14 pMLC
200 µm
B
No stimulation
P < 0.005
P < 0.005
% of alveoli
120
90
60
30
0
Oxytocin
P > 0.005
Nil
Partial†
Full
pMLC+ cells
per alveolus

Fig. S3.

Distribution of pMLC-positive cells. (**A**) Maximum intensity *z*-projections [0-80.5 μm (left), 0-140 μm (right)] of cleared mammary tissue immunostained with K14 to reveal basal cells and pMLC to show areas of recent contractile activity (prior to fixation). Asterisk shows a cluster of $pMLC^{+}$ cells in lactating mammary tissue stimulated with OT (85 nM) for 5 min. (**B**) Percent of alveoli containing no pMLC positive cells versus those containing partial (†1 or more positive cell) or that are fully-populated with pMLC positive cells. N = 3; one-way ANOVA with Bonferroni post-tests.

Figure S4

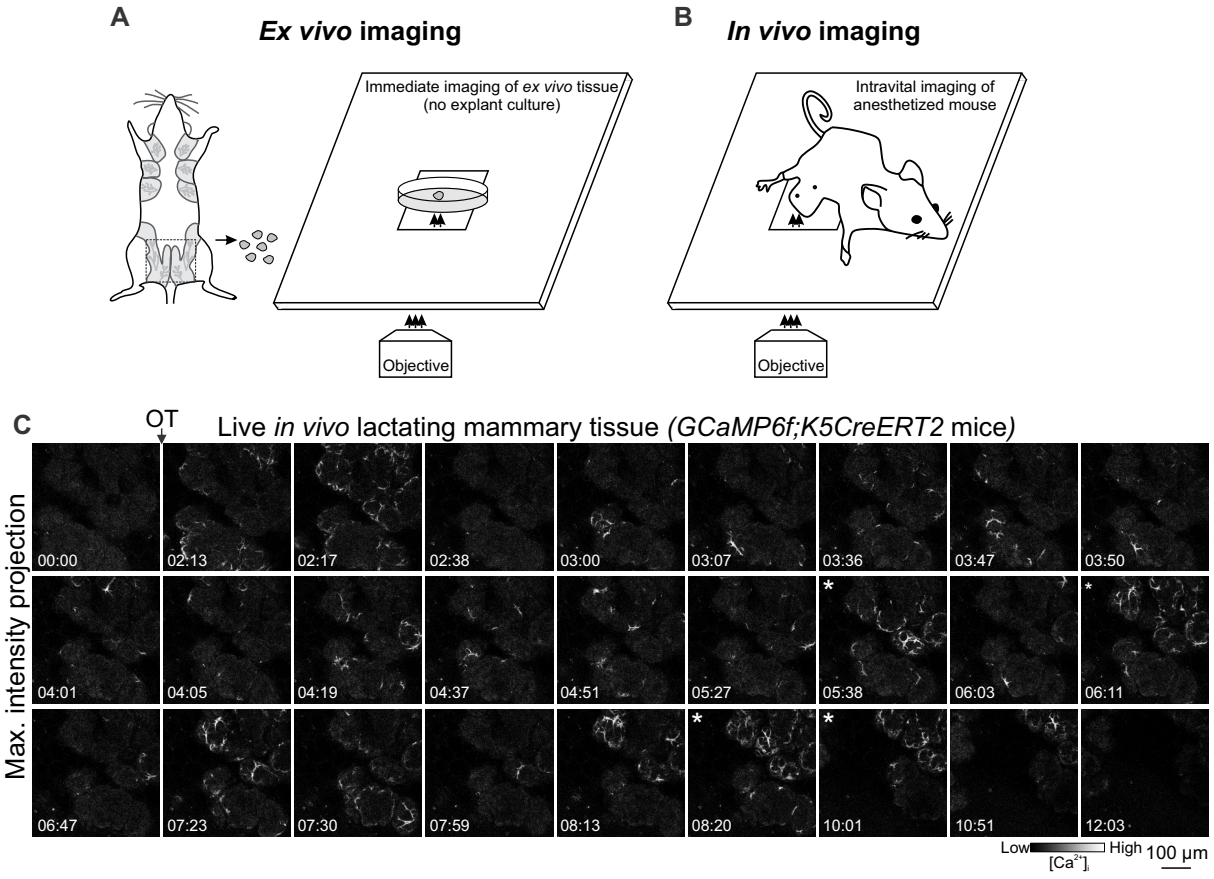
A
Ex vivo imaging
Immediate imaging of ex vivo tissue
(no explant culture)
Objective
B
In vivo imaging
Intravital imaging of
anesthetized mouse
Objective
C
OT
Live in vivo lactating mammary tissue (GCaMP6f;K5CreERT2 mice)
Max. intensity projection
00:00
02:13
02:17
02:38
03:00
03:07
03:36
03:47
03:50
04:01
04:05
04:19
04:37
04:51
05:27
05:38
06:03
06:11
06:47
07:23
07:30
07:59
08:13
08:20
10:01
10:51
12:03
Low
High
[Ca2+]i
100 µm

Fig. S4.

Intravital imaging of OT responses. Imaging set up for *ex vivo* (**A**) and *in vivo* (**B**) tissue imaging. (**C**) 3D *in vivo* time-lapse imaging of mammary tissue from a *GCaMP6f;K5CreERT2* lactating mouse injected (i.p.) with OT (2.2 U) between 01:10-01:26 (min:s). Images show maximum intensity *z*-projection 36 μm through tissue. Asterisks show coordinated firing. See also Movie S2. N = 3.

Figure S5

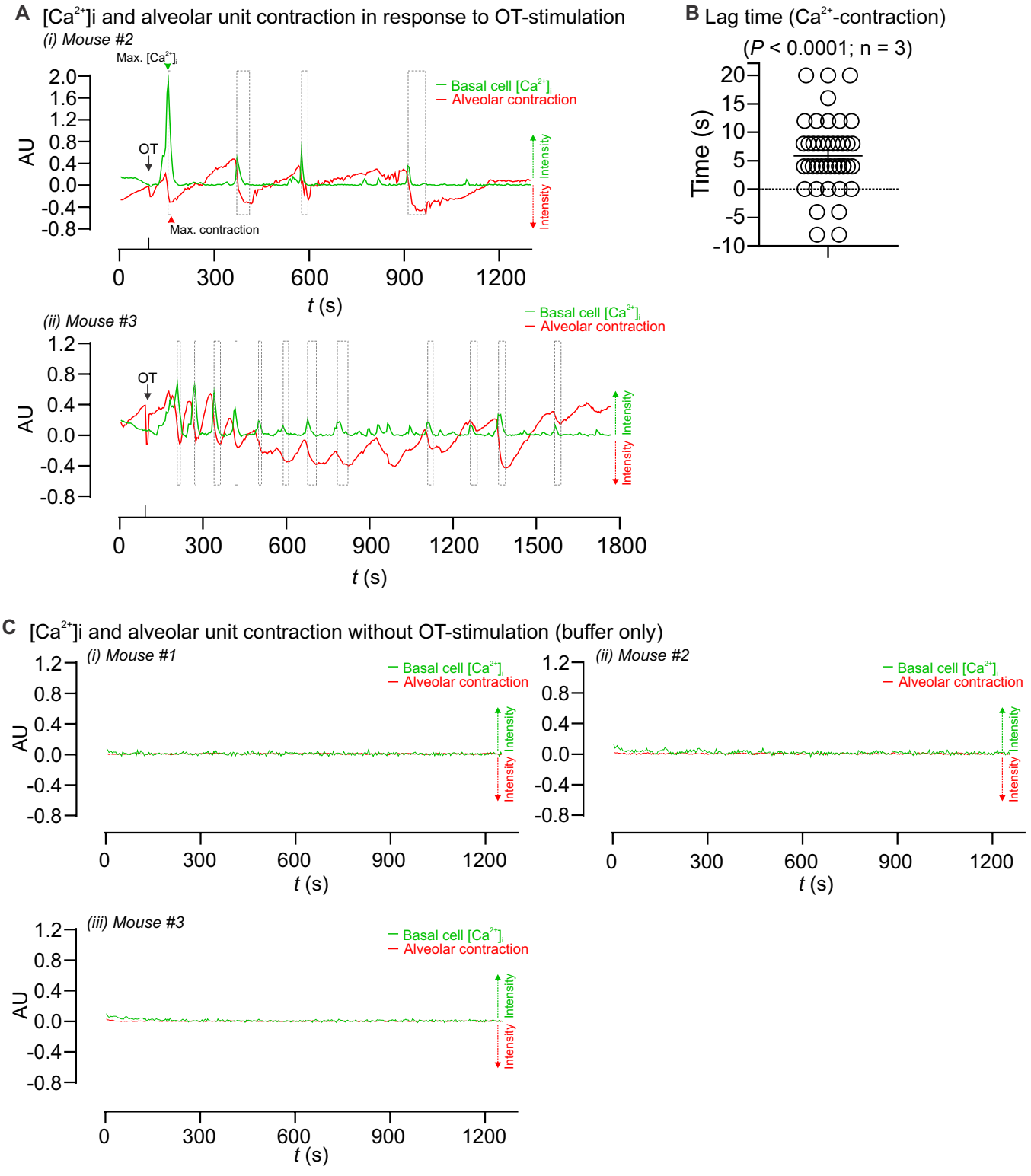
A [Ca2+]i and alveolar unit contraction in response to OT-stimulation
(i) Mouse #2
Max. [Ca2+]i
Basal cell [Ca2+]i
Alveolar contraction
OT
Max. contraction
Intensity
AU
t (s)
(ii) Mouse #3
B Lag time (Ca2+-contraction)
(P < 0.0001; n = 3)
Time (s)
C [Ca2+]i and alveolar unit contraction without OT-stimulation (buffer only)
(i) Mouse #1
(ii) Mouse #2
(iii) Mouse #3

Fig. S5.

Temporal relationship between $[Ca^{2+}]_i$ responses and alveolar unit contraction. (**A**) Additional examples (related to Fig. 1) showing $[Ca^{2+}]_i$ responses (green) and alveolar unit contractions (red) in lactating mammary tissue from *GCaMP6f;K5CreERT2* mice. $[Ca^{2+}]_i$ measurements are $\Delta F/F_0$. Alveolar unit contractions are shown by negative deflection (reduction in the intensity of the red fluorescence due to displacement of the alveolar unit). Boxes align with the peak $[Ca^{2+}]_i$ response (left) and the peak contractile response (right). (**B**) Lag time (measured as 30% deviation from baseline) of contraction after the $[Ca^{2+}]_i$ response. Graph shows mean ± S.E.M. $P < 0.0001$ (Wilcoxon test against a null hypothesis of no contraction lag). $P = 0.0023$ (binomial test of random chance of positive and negative lags). (**C**) $[Ca^{2+}]_i$ responses (green) and alveolar unit contractions (red) in lactating mammary tissue from *GCaMP6f;K5CreERT2* mice treated with buffer only (physiological salt solution). N = 3 mice. AU, arbitrary unit.

Figure S6

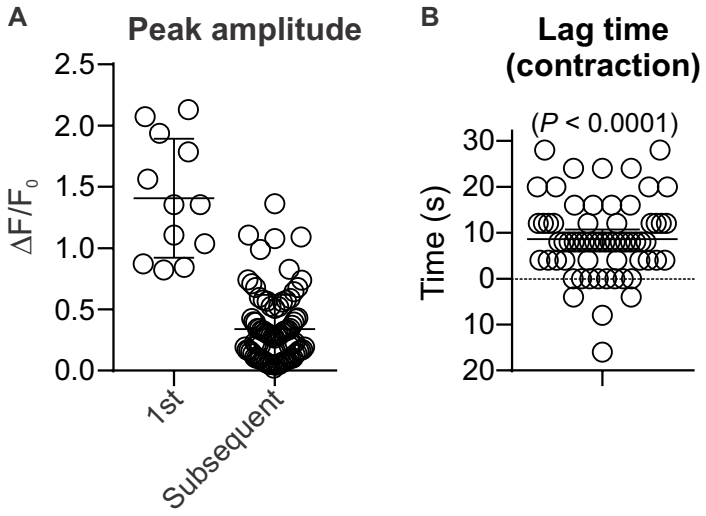
A
Peak amplitude
2.5
2.0
1.5
1.0
0.5
0.0
ΔF/F0
1st
Subsequent
B
Lag time
(contraction)
(P < 0.0001)
30
20
10
0
10
20
Time (s)

Fig. S6. Quantitative analyses of volumetric data from GCaMP6f-TdTom;K5CreERT2 model. (**A**) Peak amplitude of $[Ca^{2+}]_i$ oscillations in response to OT (85 nM). Graph shows mean ± S.D. (**B**) Lag time (measured as 30% deviation from baseline) of contraction after the $[Ca^{2+}]_i$ response. Graph shows mean and 95% confidence interval. $P < 0.0001$ (Wilcoxon test against a null hypothesis of no contraction lag). $P < 0.0001$ (binomial test of random chance of positive and negative lags). N = 3 mice.

Figure S7

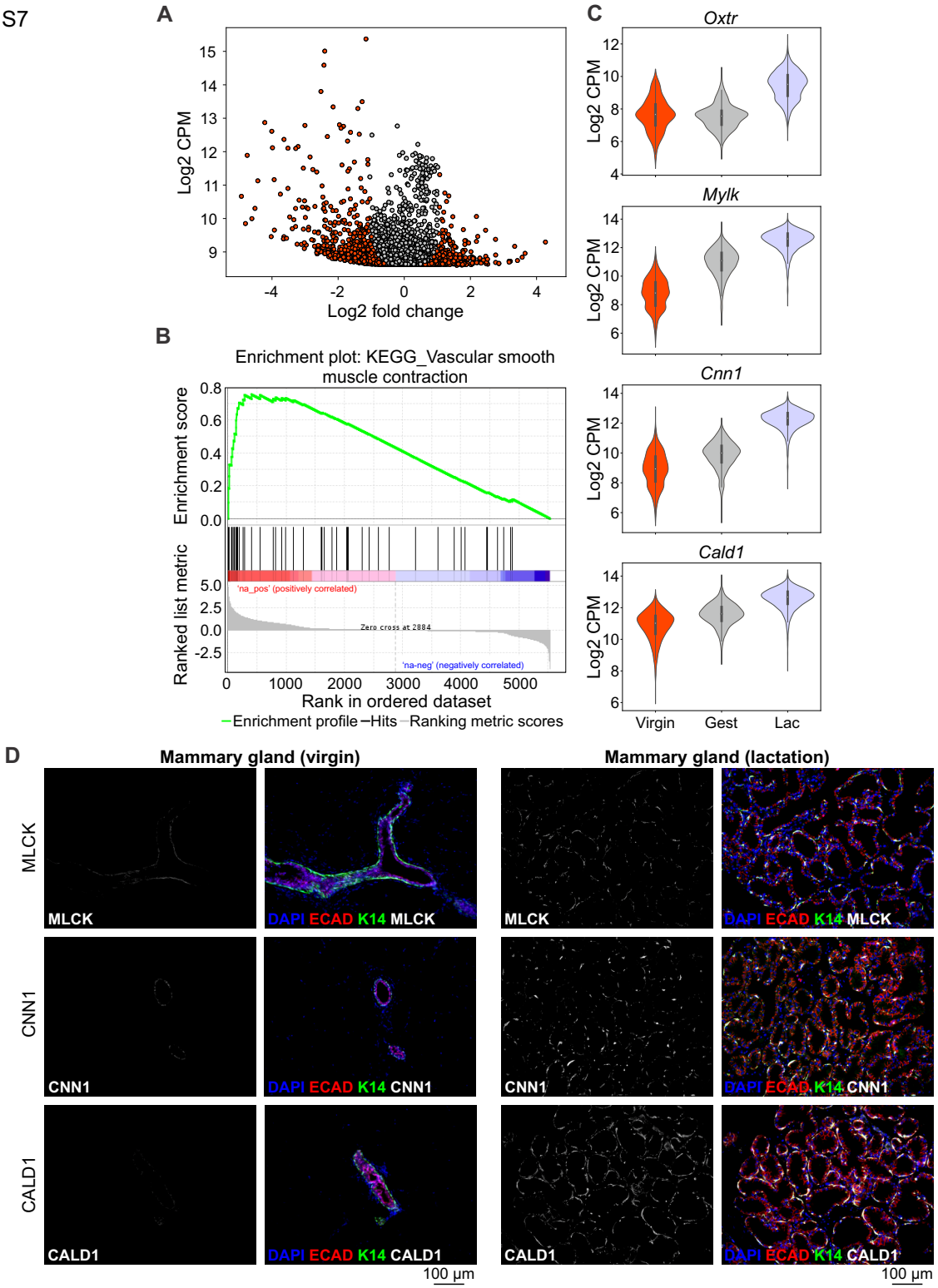
A
Log2 CPM
Log2 fold change
B
Enrichment plot: KEGG_Vascular smooth muscle contraction
Enrichment score
Ranked list metric
'na_pos' (positively correlated)
Zero cross at 2884
'na-neg' (negatively correlated)
Rank in ordered dataset
Enrichment profile Hits Ranking metric scores
C
Oxtr
Mylk
Cnn1
Cald1
Log2 CPM
Virgin
Gest
Lac
D
Mammary gland (virgin)
Mammary gland (lactation)
MLCK
CNN1
CALD1
DAPI ECAD K14 MLCK
DAPI ECAD K14 CNN1
DAPI ECAD K14 CALD1
100 µm

Fig. S7.

Upregulation of the contraction toolkit in basal cells during pregnancy and lactation. (**A**) Volcano plot showing differential expression (red dots; FDR < 0.05) from single cell RNA sequencing data [Basal-Virgin vs. Basal-Lac (lactation) clusters; Bach et al., (2017) Nat Commun]. (**B**) Genes in the KEGG vascular smooth muscle contraction pathway showed significant enrichment in Basal-Lac vs. Basal-Virgin by GSEA using MSigDB curated gene sets. (**C**) Frequency distribution of expression values from Basal-Virgin, Basal-Gest (gestation) and Basal-Lac clusters shown as a violin plot for each gene. Expression (*y*-axis) shown as log2 counts per million (CPM); width reflects the distribution of values on the *y*-axis. (**D**) Immunohistochemical staining for myosin light chain kinase (MLCK), calponin (CNN1) and caldesmon (CALD1) in mammary tissue isolated from virgin and lactating wild-type mice. E-cadherin (red) shows the luminal cell lineage; K14 (green) shows the basal cell lineage. Nuclei are stained with DAPI (blue); n = 3 mice.

Figure S8

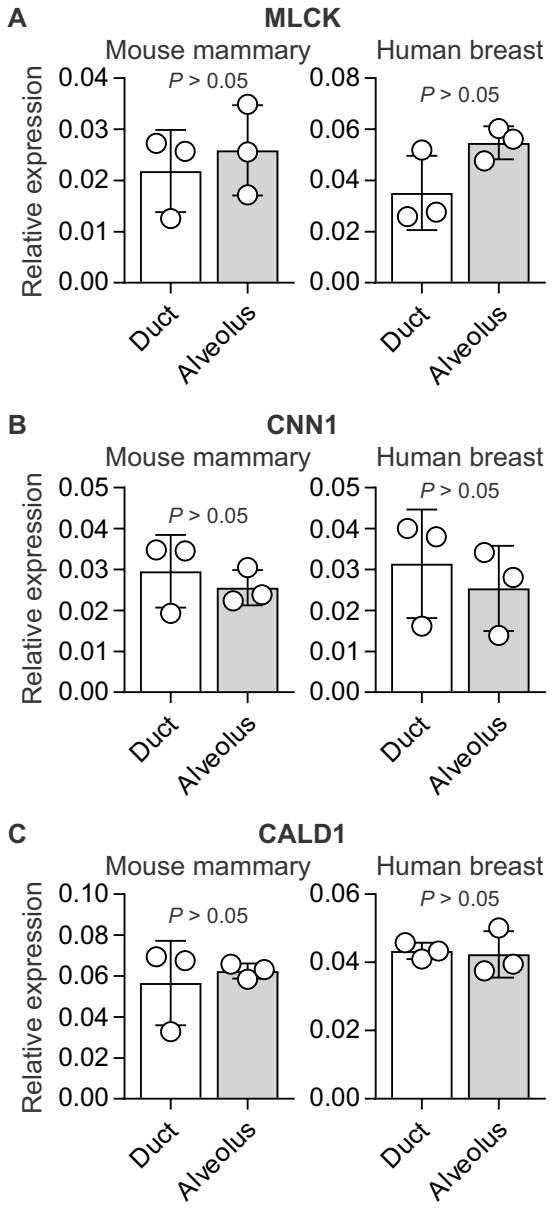
A
MLCK
Mouse mammary
Human breast
Relative expression
P > 0.05
P > 0.05
0.04
0.03
0.02
0.01
0.00
0.08
0.06
0.04
0.02
0.00
Duct
Alveolus
Duct
Alveolus
B
CNN1
Mouse mammary
Human breast
Relative expression
P > 0.05
P > 0.05
0.05
0.04
0.03
0.02
0.01
0.00
0.05
0.04
0.03
0.02
0.01
0.00
Duct
Alveolus
Duct
Alveolus
C
CALD1
Mouse mammary
Human breast
Relative expression
P > 0.05
P > 0.05
0.10
0.08
0.06
0.04
0.02
0.00
0.06
0.04
0.02
0.00
Duct
Alveolus
Duct
Alveolus

Fig. S8.

Quantitative assessment of the expression of contractile proteins in ductal and alveolar basal cells. Assessment of relative intensity of (**A**) MLCK, (**B**) CNN1 and (**C**) CALD1 in ductal and alveolar basal cells from mouse and human. Related to Fig. 3A-B. Graphs show individual values and mean ± S.D. $P > 0.05$, Student's t-test. N = 3.

Figure S9

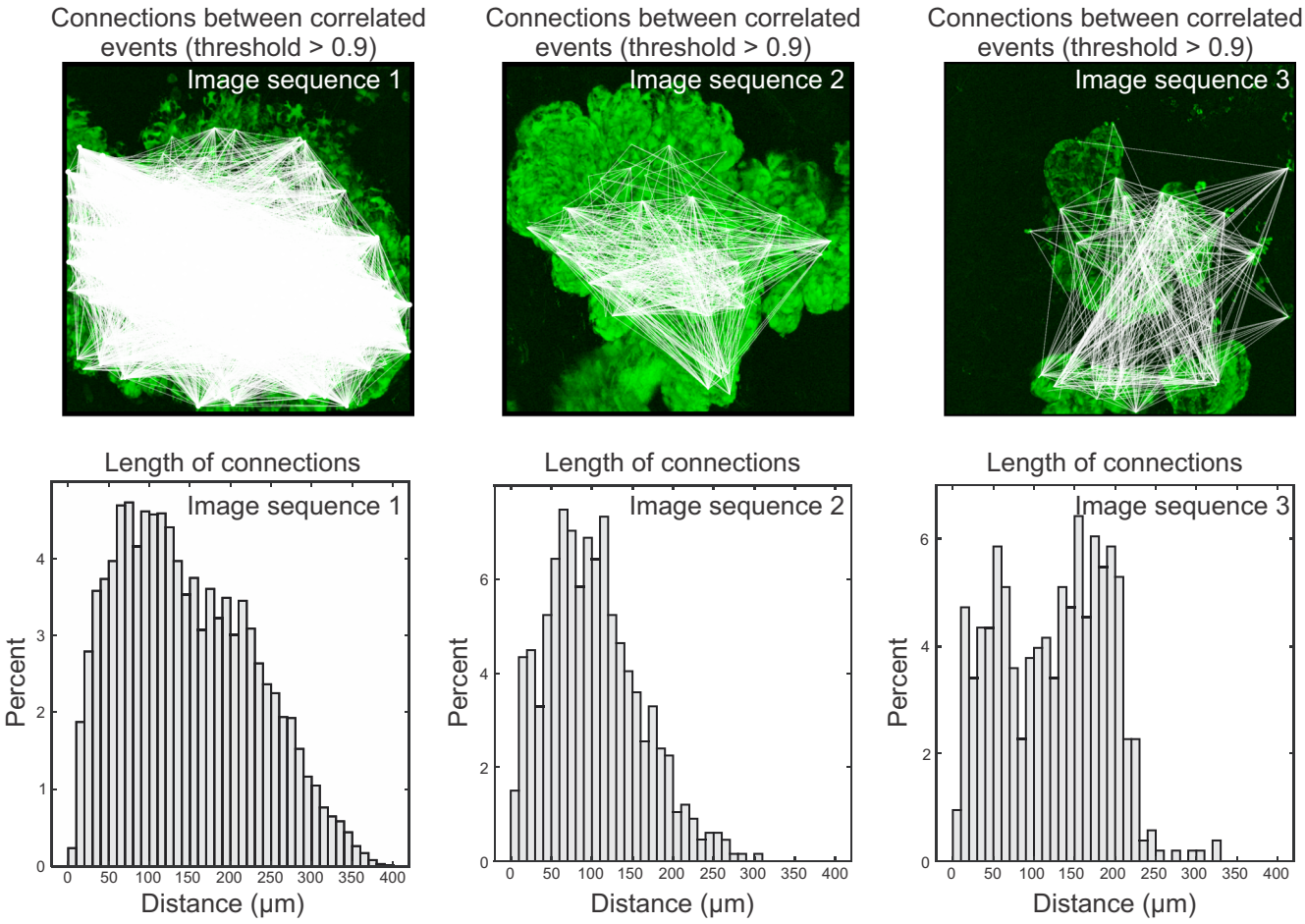
Connections between correlated events (threshold > 0.9)
Image sequence 1
Connections between correlated events (threshold > 0.9)
Image sequence 2
Connections between correlated events (threshold > 0.9)
Image sequence 3
Length of connections
Image sequence 1
Percent
Distance (μm)
Length of connections
Image sequence 2
Percent
Distance (μm)
Length of connections
Image sequence 3
Percent
Distance (μm)

Fig. S9

Tissue coordination in mammary tissue from pregnant (15.5-16.5 d.p.c.) GCaMP6f-TdTom;K5CreERT2 mice. Graph theory showing connection between highly correlated events (>0.9, white) and the length of connections.

Figure S10

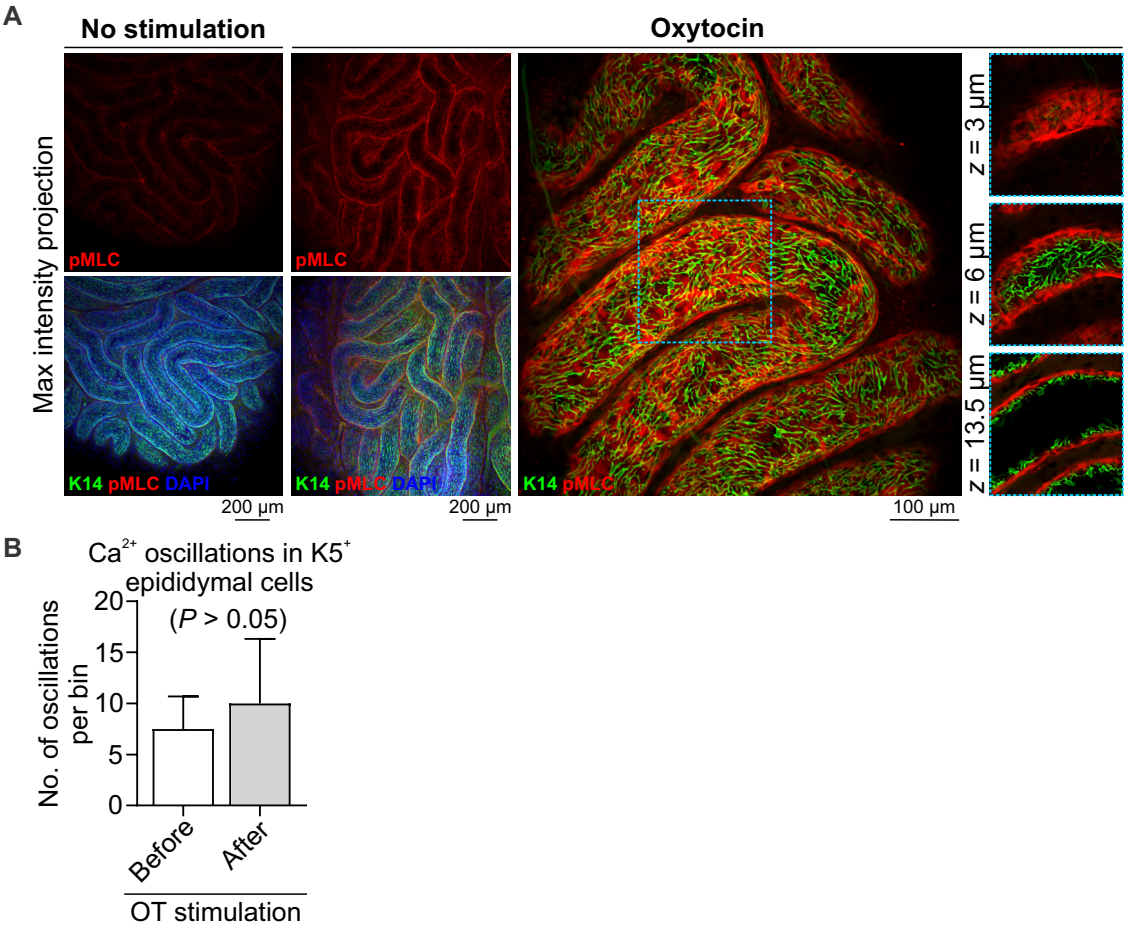
A
No stimulation
Oxytocin
Max intensity projection
pMLC
pMLC
K14 pMLC DAPI
K14 pMLC DAPI
K14 pMLC
z = 3 µm
z = 6 µm
z = 13.5 µm
200 µm
200 µm
100 µm
B
Ca2+ oscillations in K5+ epididymal cells
(P > 0.05)
No. of oscillations per bin
20
15
10
5
0
Before
After
OT stimulation

Fig. S10.

Detection of pMLC-positive cells and $[Ca^{2+}]_i$ oscillations in epididymal tissue. (**A**) Maximum intensity *z*-projection of cleared epididymal tissue immunostained with K14 (green) and pMLC (red). Tissue was stimulated with OT (850 nM) 20 min prior to fixation, as indicated. Nuclei (DAPI) are blue; representative of n = 3 mice. (**B**) Number of $[Ca^{2+}]_i$ oscillations in K5-expressing epididymal cells before and after OT stimulation (850 nM). Graph shows mean ± S.E.M.; $P > 0.05$ (paired t-test); n = 4 mice.

Figure S11

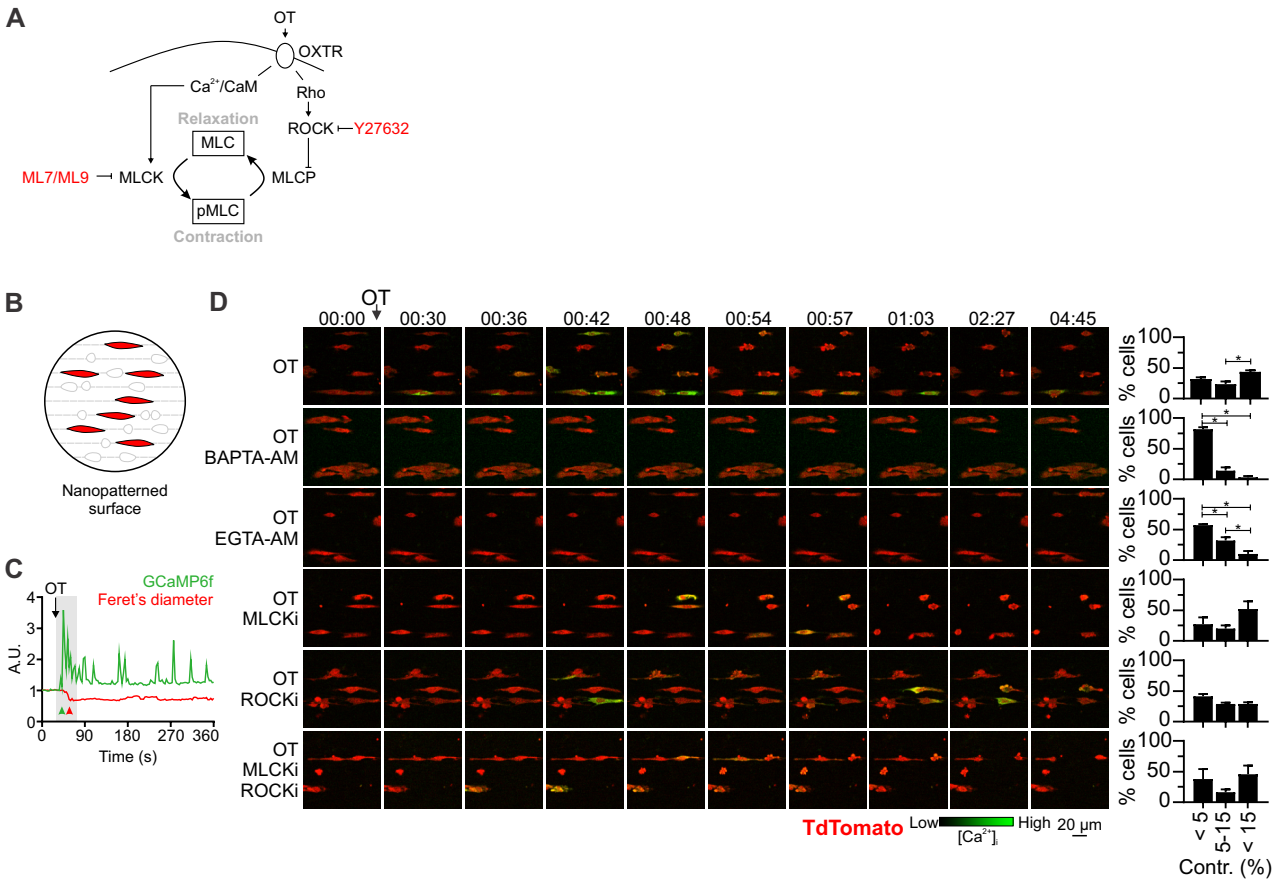
A
OT
OXTR
Ca2+/CaM
Rho
Relaxation
MLC
ROCK
Y27632
ML7/ML9
MLCK
MLCP
pMLC
Contraction
B
Nanopatterned surface
C
OT
GCaMP6f
Feret's diameter
A.U.
Time (s)
D
OT
00:00
00:30
00:36
00:42
00:48
00:54
00:57
01:03
02:27
04:45
OT
OT BAPTA-AM
OT EGTA-AM
OT MLCKi
OT ROCKi
OT MLCKi ROCKi
TdTomato
Low
High
[Ca2+]i
20 μm
% cells
< 5
5-15
< 15
Contr. (%)

Fig. S11.

Pharmacological inhibitors of contractile machinery. (**A**) Schematic representation of contractile pathways in smooth muscle cells and (**B**) the assay developed to assess *in vitro* contractile responses. (**C**) First phase (gray box) Ca^{2+}-contraction coupling in primary cells *in vitro*. (**D**) 2D time-lapse imaging of GCaMP6f-TdTomato dual positive cells in response to OT (0.85 nM, 00:27), or with OT in cells loaded with the intracellular Ca^{2+} chelators (BAPTA-AM and EGTA-AM), MLCKi (ML-7), ROCKi (Y27632) or a combination of MLCKi and ROCKi. Graphs show average (± SEM) percent cells in each bin [<5%, 5-15%, >15% reduction in Feret's diameter (contr.)]; * $P < 0.05$ one-way ANOVA with Bonferroni post-tests; 80-150 cells analyzed for each treatment from n = 3 mice.

Figure S12

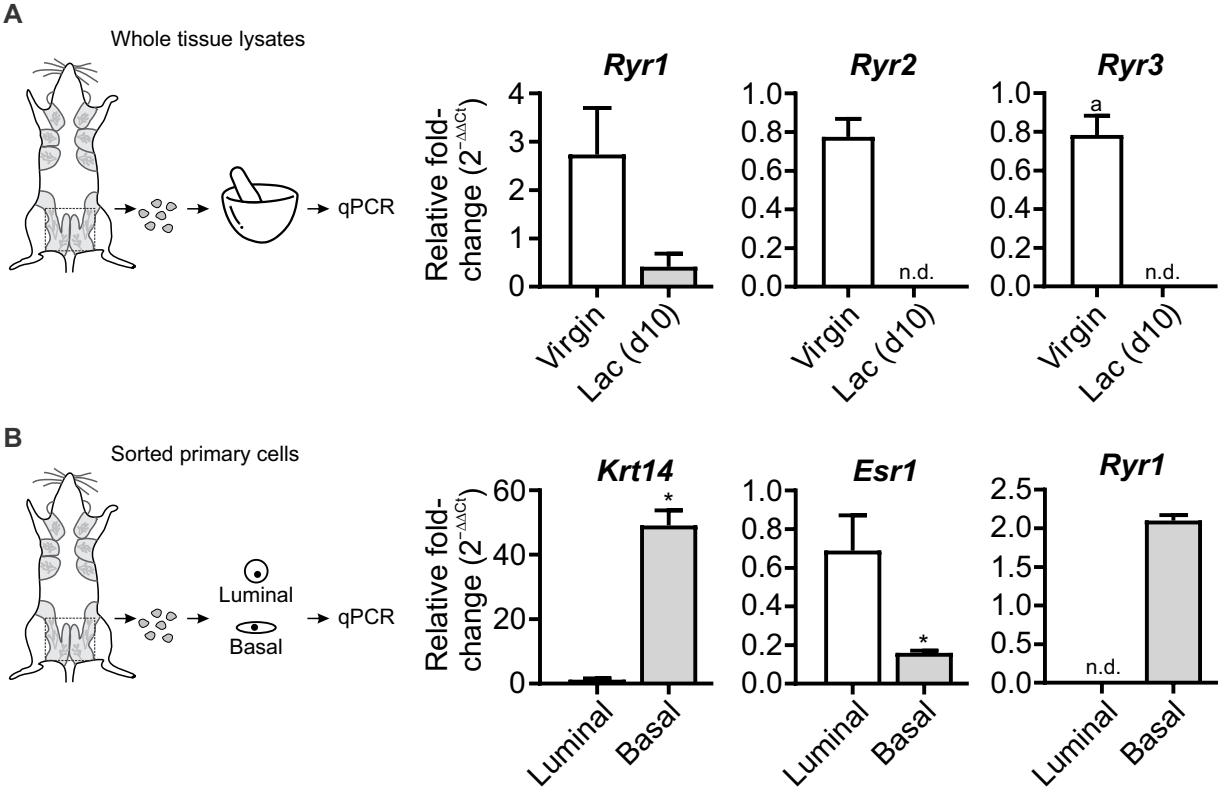
A
Whole tissue lysates
qPCR
Ryr1
Ryr2
Ryr3
Relative fold-change ($2^{-\Delta\Delta Ct}$)
a
n.d.
n.d.
Virgin
Lac (d10)
B
Sorted primary cells
Luminal
Basal
qPCR
Krt14
Esr1
Ryr1
*
*
n.d.
Luminal
Basal

Fig. S12.

mRNA levels of ryanodine receptors. (**A**) *Ryr1*, *Ryr2* and *Ryr3* expression in lysates prepared from whole mammary tissue (including luminal, basal and stromal cells) dissected from virgin or lactating animals (n = 4 mice). (**B**) *Krt14*, *Esr1* and *Ryr1* levels in freshly sorted luminal and basal cells (n = 3 mice). Graphs show mean ± SEM; * $P < 0.05$ (Student's t-test); n.d., not detected. *Ryr2* and *Ryr3* transcripts were either not detected or detected at very low levels in only a fraction of samples from both luminal and basal cells.

Figure S13

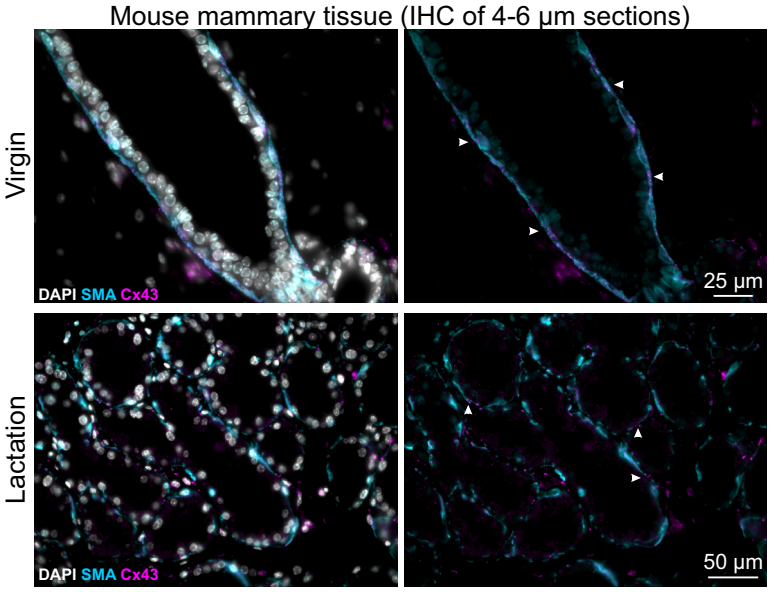
Mouse mammary tissue (IHC of 4-6 µm sections)
Virgin
Lactation
DAPI SMA Cx43
DAPI SMA Cx43
25 µm
50 µm

Fig. S13.

Cx43 expression (2D tissue sections). Cx43 immunostaining (magenta) in virgin and lactating mammary tissue. SMA (cyan) shows the basal cell lineage. Nuclei are stained with DAPI (gray).

Supplementary Movie Legends

Movie S1.
OT response in live mammary tissue isolated from a lactating *GCaMP6f;K5CreERT2* mouse. GCaMP6f (green) and CellTracker™ (red). OT was added at 01:33 (min:s). Total movie length is 29:30 (min:s). Related to Fig. 1.

Movie S2.
Intravital imaging of OT response in a lactating *GCaMP6f;K5CreERT2* mouse. OT was injected between 01:10-01:26 (min:s) and exhibits a similar (albeit faster) response to that seen acute *ex vivo* tissue (Movie S1). Total movie length is 29:30 (min:s). Related to Fig. S4.

Movie S3.
OT response in live mammary tissue isolated from a lactating *GCaMP6f-TdTom;K5CreERT2* mouse. GCaMP6f (green) and TdTomato (red). OT was added at 01:09 (min:s). Total movie length is 23:03 (min:s). Related to Fig. 2.

Movie S4.
OT response in live mammary (alveolar) tissue isolated from a pregnant (15.5-16.5 d.p.c.) *GCaMP6f-TdTom;K5CreERT2* mouse. GCaMP6f (green) and TdTomato (red). OT was added at 00:38 (min:s). Total movie length is 25:08 (min:s).

Movie S5.
OT response in live mammary (alveolar) tissue isolated from a pregnant (15.5-16.5 d.p.c.) *GCaMP6f-TdTom;K5CreERT2* mouse. Tissue was incubated in Ca^{2+} free buffer prior to imaging. Extracellular Ca^{2+} was added back at a final concentration of 1 mM (free Ca^{2+}), as indicated. Total movie length is 29:55 (min:s). Related to Fig 2.

Movie S6.
OT response in live mammary (ductal) tissue isolated from a pregnant (15.5-16.5 d.p.c.) *GCaMP6f-TdTom;K5CreERT2* mouse. GCaMP6f (green) and TdTomato (red). OT was added at 01:15 (min:s), as indicated. Total movie length is 26:13 (min:s). Related to Fig. 3.

Movie S7.
OT response in live mammary (ductal) tissue isolated from a lactating *GCaMP6f-TdTom;K5CreERT2* mouse. GCaMP6f (green) and TdTomato (red). OT was added approximately 00:45 (min:s) prior to imaging. Total movie length is 26:13 (min:s). Related to Fig. 3.

Movie S8.

OT response in live lacrimal tissue isolated from a *GCaMP6f-TdTom;K5CreERT2* mouse. GCaMP6f (green) and TdTomato (red). OT was added at 00:45 (min:s), as indicated. Total movie length is 15:55 (min:s). Related to Fig. 4.

Movie S9.

OT response in live epididymal tissue isolated from a *GCaMP6f-TdTom;K5CreERT2* mouse. GCaMP6f (green) and TdTomato (red). OT was added at 01:38 (min:s), as indicated. Total movie length is 25:48 (min:s). Related to Fig. 4.

Movie S10.

Tissue contraction in response to pharmacological inhibitors. From top to bottom: uterus, epididymis, bladder and mammary gland loaded with CellTracker™. From Left to right: control, MLCKi+ROCKi, MLCKi+ROCKi+PKCi+CaMKIIi. Uterus and mammary tissue was stimulated with OT (85 nM). Epididymal tissue was stimulated with OT (850 nM). Bladder tissue was stimulated with carbachol (10 μM) at the commencement of imaging. Related to Fig. 5.

Movie S11.

OT response in live primary cells isolated from a pregnant (15.5-16.5 d.p.c.) *GCaMP6f-TdTom;K5CreERT2* mouse and grown on a nanopatterned surface. OT was added at 00:27 (min:s), as indicated. Total movie length is 06:00 (min:s). Related to Fig. S11.

Movie S12.

OT response in live primary cells isolated from a pregnant (15.5-16.5 d.p.c.) *GCaMP6f-TdTom;K5CreERT2* mouse, grown on a nanopatterned surface and pre-treated with BAPTA-AM for 30 min. OT was added at 00:27 (min:s), as indicated. Total movie length is 06:00 (min:s). Related to Fig. S11.

Movie S13.

OT response in live mammary tissue isolated from a lactating *GCaMP6f;K5CreERT2* mouse. Tissue was pre-treated with dantrolene (20 μM) for approx. 5 h. GCaMP6f (green) and TdTomato (red). OT was added at 01:53 (min:s). Total movie length is 32:51 (min:s). Related to Fig. 6.

Movie S14.

OT response in live mammary tissue isolated from a lactating *GCaMP6f;K5CreERT2* mouse. Tissue was pre-treated with ryanodine (100 μM) for approx. 5 h. GCaMP6f (green) and TdTomato (red). OT was added approx. 12 min prior to imaging. Total movie length is 12:14 (min:s).

Movie S15.

The effect of nifedipine on tissue synchronization promoted by dantrolene. Tissue from a pregnant *GCaMP6f-TdTom;K5CreERT2* mouse was pre-treated with dantrolene and stimulated with OT (85 nM) approx. 12 min prior to imaging. Nifedipine (20 μM) was added at 21:30 (min:s), as indicated. Total movie length is 29:55 (min:s). Related to Fig. 6.

Supplementary Methods

Mice

Animals were kept in a Specific Pathogen Free facility under a 12:12 h light-dark cycle in individually ventilated cages. Food and water were available *ad libitum* and standard enrichment provided. All strains were purchased and maintained on a C57BL6 background. *K5CreERT2* mice (B6N.129S6(Cg)-Krt5$^{tm1.1(cre/ERT2)Blh}$/J, stock no. 029155) and *Lck-GCaMP6f-fl* mice (C57BL/6N-Gt(ROSA)26Sor$^{tm1(CAG-GCaMP6f)Khakh}$/J, stock no. 029626) were purchased from The Jackson Laboratory (Bar Harbor, ME). *TdTomato-fl* mice (B6.Cg-*Gt(ROSA)26Sor*$^{tm9(CAG-tdTomato)Hze}$/J, stock no. 007909) were a kind gift from Prof. Ian Frazer (University of Queensland). *GCaMP6f-fl* mice (B6J.Cg-*Gt(ROSA)26Sor*$^{tm95.1(CAG-GCaMP6f)Hze}$/MwarJ) were a kind gift from Dr James W. Putney Jr (National Institute of Environmental Health Sciences). C57BL6/J mice were obtained from the Animal Resources Centre (Western Australia). All Cre-expressing lines were maintained as heterozygotes.

Genotyping was performed on mouse toe or ear DNA using the following primers: to distinguish *K5-CreERT2* 5'-GCA AGA CCC TGG TCC TCA C-3', 5'-GGA GGA AGT CAG AAC CAG GAC-3', 5'-ACC GGC CTT ATT CCA AGC-3' (wildtype 322 bp, mutant 190 bp); and to distinguish *TdTomato-fl, GCaMP6f-fl* and *Lck-GCaMP6f-fl* 5'-CTC TGC TGC CTC CTG GCT TCT-3', 5'-CGA GGC GGA TCA CAA GCA ATA-3' and 5'-TCA ATG GGC GGG GGT CGT T-3' (wildtype 330 bp, mutant 250 bp).

To induce expression of GCaMP6f and TdTomato in K5-positive cells, female mice were administered tamoxifen (1.5 mg) (Sigma Aldich, T5648) diluted in sunflower oil (Sigma Aldrich, S5007) and ethanol (10%) via intraperitoneal injection at 4-weeks of age. A further 2-3 tamoxifen injections were administered every second day on alternating sides at 8-weeks of age, providing a total dose of 4.5-6 mg per mouse. A 4-6-week washout period was observed before mating. Male mice were injected with 4 × 1.5 mg tamoxifen injections every second day at 8-weeks of age (total dose 6 mg per mouse). Female experimental mice were mated in pairs or trios with wildtype sires. To obtain mammary tissue during gestation, sires were removed after observation of a copulation plug and mammary tissue harvested 15.5-16.5 d.p.c (days post coitus). To obtain lactating tissue, sires were removed prior to littering and female mice were allowed to nurse for 8-14 days (peak lactation).

Human subjects

Healthy tissue biopsies from consented lactating women (25-33 years old) were obtained from the Susan G. Komen Tissue Bank at the IU Simon Cancer Center (1). Tissue donors were recruited under a protocol approved by the Indiana University Institutional Review Board (IRB protocol number 1011003097) and according to The Code of Ethics of the World Medical Association (Declaration of Helsinki), with site-specific approval from the Mater Misericordiae Ltd Human Research Ethics Committee. Breast biopsies were fixed in formalin and paraffin

embedded as per standard protocols. Lactating samples were collected from women who were actively breastfeeding at the time of tissue donation (at least once per day). Donors included in this study had been breastfeeding for 6 to 23 months prior to tissue donation.

Immunohistochemistry

IHC was performed based on a previously published protocol (2). Briefly, formalin-fixed paraffin embedded mouse and human slides were deparaffinized in xylene and rehydrated in a reducing ethanol series. Tissue was permeabilized in phosphate buffered saline (PBS) containing triton X-100 (0.5%). Heat-induced epitope retrieval was performed in sodium citrate (0.01 M, pH 6) for 11 min at 110°C using a NxGen Decloaking Chamber. Slides were blocked in PBS containing normal goat serum (10%) and triton X-100 (0.05%) for 1 h. Primary antibodies were incubated overnight at 4°C in a humidified chamber. The following primary antibodies were used in this study: rabbit anti-SMA (Abcam, ab5694, 1:600), rabbit anti-MLCK (Sigma Aldrich, HPA031677, 1:700-1:1000), rabbit anti-CNN1 (Abcam, ab46794, 1:700-1:1000), rabbit anti-CALD1 (Sigma Aldrich, HPA008066, 1:200), mouse anti-E-cadherin (BD Biosciences, 610182, 1:200-1:400), chicken anti-K14 (BioLegend, 906004, 1:200-1:400) and rabbit anti-Cx43 (Abcam, ab11370, 1:1000). Secondary antibodies were incubated for 1 h at room temperature. The following secondary antibodies were used in this study (1:500): goat anti-rabbit Alexa Fluor 647 (ThermoFisher Scientific, A21236), goat anti-mouse Alexa Fluor 555 (ThermoFisher Scientific, A32727) and goat anti-chicken Alexa Fluor 488 (ThermoFisher Scientific, A11039). Nuclei were stained with DAPI dilactate (625 ng/mL) for 10 min at room temperature and tissue was imaged on an Olympus BX63F upright epifluorescence microscope. For quantification of IHC images exposure times were kept consistent between samples and brightness and contrast adjustments were uniformly applied.

Tissue clearing

Mammary tissue was dissected, spread on foam biopsy pads and optimally fixed in neutral buffered formalin (NBF, 10%) for 3-9 h (according to size) at room temperature. Lacrimal and epididymal tissue was dissected and fixed in NBF for 4-7 h. Pre-stimulation with OT [85 nM (lacrimal and mammary), 850 nM (epididymis), 2-10 min] was performed on live tissue prior to fixation, as indicated. Tissue clearing was performed on fixed tissue using a modified CUBIC protocol (3, 4), except for studies examining Cx43 and the membrane targeted fluorescent protein, which used SeeDB (5).

For CUBIC clearing, tissue was immersed in CUBIC Reagent 1A [urea (10% w/w), Quadrol® (5% w/w), triton X-100 (10% w/w), NaCl (25 mM) in distilled water] for 2-3 days at 37°C, washed in PBS and blocked overnight at 4°C in PBS containing normal goat serum (10%) and triton X-100 (0.5%). Tissue was incubated in primary antibodies diluted blocking buffer at 4°C for 4 days. The following primary antibodies and dilutions were used for wholemount immunostaining in this study: rabbit anti-SMA (1:300), chicken anti-K14 (1:200), rabbit anti-pMLC (Abcam,

ab2480, 1:200) and chicken anti-GFP (Abcam, ab13970, 1:1000-1:2000). Secondary antibodies (Life Technologies) are listed above and used 1:500, incubated for 2 days at 4°C for wholemount immunostaining. Nuclei were stained with DAPI dilactate (5 μg/mL) for 2-3 h at room temperature. Washing was performed in PBS after primary and secondary antibody incubations (3 × 1 h). Tissue was placed in modified CUBIC Reagent 2 [sucrose (44% w/w), urea (22% w/w), triethanolamine (9% w/w), triton X-100 (0.1% v/w) in distilled water] at 37°C and imaged within 1-7 days (4, 6). Tissue was imaged in CUBIC Reagent 2 using an Olympus FV3000 laser scanning confocal microscope with UPLSAPO 10×/0.4, UPLSAPO 20×/0.75 and UPLFLN 40×/0.75 objective lenses. For SeeDB clearing, tissue was blocked overnight at 4°C in PBS containing BSA (10%) and triton X-100 (1%) and incubated in primary antibodies diluted blocking buffer at 4°C for 4 days [chicken anti-GFP, rabbit anti-SMA or rabbit anti-Cx43 (1:200)]. Tissue was washed and incubated in secondary antibodies and DAPI as described above, before moving through increasing fructose solutions (3). Imaging depth (*z*) is recorded from the start of the image sequence, typically 50-150 μm through the cleared structure. Visualization and image processing was performed in Imaris (v9.2.1) or ImageJ (v1.52e, National Institutes of Health) (7, 8). Denoising of 3D image stacks was performed as previously described (9).

Primary cell imaging

Abdominal and inguinal mammary glands were dissected from pregnant *GCaMP6f-TdTom;K5CreERT2* mice (15.5-16.5 d.p.c.), lymph nodes removed and mammary tissue finely chopped. Cells were isolated using adapted published protocols (10, 11). Briefly, diced tissue was incubated at 37°C with gentle rocking in DMEM/F-12 (with L-glutamine and HEPES, ThermoFisher Scientific 11330032) supplemented with collagenase (Roche, 11088793001, 1 mg/mL) and hyaluronidase (Sigma Aldrich, H3506, 100 U/mL). Cells were disrupted every 30 min using a transfer pipette. After 3 h the tube was removed from the incubator, cells were further disrupted by pipetting and pelleted (1500 rpm, 5 min, 4°C). The subsequent steps and washes were performed in Hank's Buffered Salt Solution with fetal calf serum (2%). Red cell lysis was performed in ammonium chloride. Pelleted cells were treated with pre-warmed trypsin (0.25%) for 1 min. Re-suspended and re-pelleted cells were then treated with pre-warmed dispase (5 mg/mL) and DNase (1 mg/mL) for 1 min, re-suspended and strained through a 40 μm cell strainer. Cells were plated in DMEM/F12 with FCS (10%) on collagen coated (50 μg/mL) NanoSurface 96-well plates (NanoSurface Biomedical ANFS-0096) and allowed to attach for at least 2.5 h.

Cells were imaged in physiological salt solution [PSS; HEPES (10 mM), KCl (5.9 mM), $MgCl_2$ (1.4 mM), NaH_2PO_4 (1.2 mM), $NaHCO_3$ (5 mM) NaCl (140 mM), glucose (11.5 mM), $CaCl_2$ (1.8 mM); pH 7.3-7.4] within 12 h from the time of sacrifice. Cells were loaded with BAPTA-AM (100 μM, ThermoFisher Scientific, B6769) and EGTA-AM (100 μM, ThermoFisher Scientific, E1219), as indicated, in complete media at 37°C for 20-40 min before imaging. Pre-treatments with ML-7 (20 μM, Abcam, Ab120848), Y27632 (10 μM, Abmole, M1817) or a combination of ML-7 and

Y27632 were performed for 10-20 min in PSS. Cells were imaged on an Olympus FV3000 inverted confocal microscope using a UPLSAPO 30×/1.05 silicone objective, resonant scanner and z-drift compensator. The rise time (T_{peak}) for GCaMP6f is approximately 80 ms; the half decay time ($T_{1/2}$) is 400 ms. Images were acquired every 3 s (< firing duration) for 6 min. Cells were stimulated with OT (0.85 nM) at 30 s; the concentration of ML-7 and Y27632 were maintained for the duration of the assay.

Primary cell contraction analysis

Images were quantified using a custom ImageJ macro for reproducibility and to eliminate bias. Briefly, cell boundaries were identified by taking the standard deviation of all movement of each cell during acquisition, thresholding and storing the selection area as an ROI. All ROIs were used for measuring intensity of red and green channels for each individual cell and time-point. For cell length measurements, cell ROIs were expanded by two pixels and the region duplicated, and converted to a binary using the Li thresholding algorithm. Individual Feret diameters were measured and recorded for each time-point and ROI. Data was output as .csv files to be further processed (size exclusion < 18 μm or >45 μm), graphed and analyzed. Of the cells that didn't contract (< 5% contr.) with OT (0.85 nM) alone, approximate 35% did not respond with $[Ca^{2+}]_i$; this submaximal OT concentration was selected because it produced cell contraction in the majority of cells, without causing complete loss of cell adhesion. Scripts are available at: https://github.com/nickcondon.

Ex vivo tissue imaging

Mammary glands and uteri were harvested from lactating wildtype, *GCaMP6f;K5CreERT2* or *GCaMP6f-TdTom;K5CreERT2* mice, diced into 3-4 mm^3 pieces and loaded with CellTracker™ Red (1.5 μM) in complete media for at least 20 min at 37°C and 5% CO_2, as indicated (12). Under these conditions CellTracker™Red preferentially stains luminal epithelial cells. Lacrimal glands (extraorbital), epididymides and bladders were isolated from wildtype or *GCaMP6f-TdTom;K5CreERT2* mice and loaded with CellTracker™ Red, as indicated. Cut (undigested) tissue pieces were anchored with netting and imaged in 35 mm imaging dishes, bathed in PSS. Tissue was stimulated with OT (85 nM, mammary, uterus and lacrimal; 850 nM epididymis) or carbachol (10 μM, bladder) in PSS. Image sequences were acquired on an Olympus FV3000 LSM using a resonant scanner and UPLSAPO 30×/1.05 silicone objective. Images were acquired every 1.8-5 s for 15-45 min, depending on tissue type and experimental conditions.

For extracellular Ca^{2+} chelation and addback experiments, tissue was incubated in Ca^{2+}-free PSS containing BAPTA (2 mM) for 40 min prior to imaging. Tissue was incubated in pharmacological inhibitors in complete media for 2-6 h prior to imaging. The following pharmacological inhibitors were used in this study: ML-9 (Tocris, 0431/10, 20 μM), Y27632 (Abmole, M1817, 20 μM), KN93 (Tocris, 12791, 20 μM), calphostin C (Tocris, 1626, 1 μM), dantrolene (Tocris, 0507, 20μM), ryanodine (Tocris, 1329, 100 μM), nifedipine (Sigma Aldrich,

N7634, 20 μM). Concentrations of all chelators and inhibitors were maintained for the duration of the imaging study. Uterine, epididymal, bladder and mammary contractions were scored on a 4-point scale by a blinded investigator.

Intravital imaging

Intravital imaging was performed on lactating mice (day 10-15) as previously described (13, 14). Nursing pups were removed and euthanized immediately prior to starting the experiment. The lactating dam was anesthetized using a combination of Zoletil® (tiletamine hydrochloride and zolazepam hydrochloride, 50 mg/kg) and xylazine (20 mg/kg) by intraperitoneal injection. Anesthesia was maintained using gaseous isofluorane (1.5%), supplied via a nose cone. Abdominal hair was removed using electronic pet clippers and Nair hair removal cream. An incision was made along the midline and hind limb to create a skin flap that extended from the abdominal midline to the spine and left the peritoneum intact. Skin was glued using Vetbond tissue adhesive to a standard microscope slide. Care was taken so that the tissue adhesive did not directly contact the mammary tissue. Vaseline and parafilm was used to protect the abdominal wall. A heat lamp was used to maintain body temperature. Blu Tack® was used to secure the slide-mounted skin flap onto the microscope stage above a #1.5 coverslip. Imaging was performed using an inverted Olympus FV3000 laser scanning microscope with a resonant scanner and UPLSAPO 30×/1.05 silicone objective. Before starting imaging, a top-up dose (30% induction dose) of injectable anesthetic was administered. Oxytocin (2.2 U) was administered via i/p injection approximately 1 min after the commencement of imaging. Vitals were monitored throughout the experiment, which was completed within 1 h from the induction of anesthesia.

qPCR

For gene expression studies from whole tissue, snap frozen virgin and lactating mammary tissue (30-100 mg) was crushed under liquid nitrogen using a mortar and pestle, lysed in Buffer RLT Plus (Qiagen) and homogenized using QIAshredder homogenizer columns (Qiagen). For gene expression studies from sorted cells, primary cells were dissociated from pregnant C57BL/6J mice as described above and prepared for flow cytometry as previously described (10). Luminal and basal cells were identified by CD49f and EpCAM expression, after exclusion of non-epithelial cells and dead cells (10). RNA isolation and purification was performed using the RNeasy Plus Mini Kit (Qiagen) with gDNA eliminator columns and cDNA was prepared using the QuantiTect Reverse Transcription kit (Qiagen). Resulting cDNA was amplified using an ABI ViiA 7 real-time PCR System, using TaqMan Fast Universal PCR Master Mix and TaqMan Gene Expression Assays, with a limit of detection set as 36 cycles. The following Gene Expression Assays were used in this study: *Ryr1* (Mm01175211_m1), *Ryr2* (Mm00465877_m1), *Ryr3* (Mm01328395_m1), *Krt14* (Mm00516876_m1) and *Esr1* (Mm00433149_m1). Relative quantification was calculated relative to 18S ribosomal RNA and analyzed using the comparative CT method (15).

Registration and analysis of live 4D tissue imaging

We used Advanced Normalization Tools (ANTs, github.com/ANTsX/ANTs) to register the red fluorescence of the live Ca^{2+} imaging to the first time point of each movie (16, 17). We used the following call on each image of the image sequence : antsRegistration -d 2 --float 1 -o [OutImg, OutImg.nii] -n WelchWindowedSinc -w [0.005,0.995] -u 1 -r [FixImg,MovImg, 1] -t rigid[0.1] - m MI[FixImg,MovImg,1,32, Regular,0.25] -c [1000x500x200x50,1e-7,5] -f 8x4x2x1 -s 2x1x1x0vox -t Affine[0.1] -m MI[FixImg,MovImg,1,32, Regular,0.25] -c [1000x500x200x50,1e-7,5] -f 8x4x2x1 -s 2x1x1x0vox -t SyN[0.05,6,0.5] -m CC[FixImg,MovImg,1,2] -c [100x500x200x50,1e-7,5] -f 8x4x2x1 -s 2x2x1x0vox -v 1. We also computed the Jacobian determinant of the resulting warps, this provided an estimate of the “strength” of the warp required to align the two images, as such it is a proxy metric of contractions. Large movements and drifts would not be included in the Jacobian determinant as these are corrected by the rigid and affine step of the registration.

The resulting warps were then applied to the GCaMP6f channel and the resulting registered movies were analyzed using MATLAB. First, we manually selected regions of interests (ROIs) and extracted the fluorescence time series of each channel. The $\Delta F/F_0$ was then computed as described previously (18), and all the GCaMP6f peaks with at least a 10% increase in $\Delta F/F_0$ (change in starting fluorescence divided by starting fluorescence), and a correlation to an example GCaMP6f trace above 0.6, were identified. The time of those peaks was used to select a time period of five frames before and ten frames after the peak in both green and red channels, these time traces were then averaged across all identified peaks within and between each mice tissue. The delay between the peaks was also evaluated with the same criteria.

To uncover any potential coordination in the firing pattern, we used a correlation-based approach. We extracted the Ca^{2+} traces from live imaging of alveolar units using the CaImAn python package (19). A correlation distance matrix was then built between all the identified ROIs, as well as a Euclidean distance matrix between their centroids, for each of the mice analyzed. These were used to either look at the probability distribution of the Euclidean distance for highly correlated (> 0.5) ROIs, or to build a weighted directed graph between these ROIs.
The same approach was used to identify sequences of synchronized activity in the Dantrolene treated tissues, we used the sequential Non-negative Matrix Factorization (seqNMF) to cluster the Ca^{2+} traces in up to 3 clusters, with a regularization factor of 0.0001 and a time window of 50 (20). The number of clusters and regularization factor value were determined empirically to minimize the dissimilarity metric and optimize the reconstruction vs x-ortho cost, see Ref (20) for details. To estimate the periodicity, or time interval between each synchronized oscillation, we measured the time between subsequent peaks of the repeated sequence identified by

seqNMF. This approach was also used to measure the velocity, by dividing the Euclidean distance between active cells with the lag each cell presents in the sequence of activation.

Gene expression analysis from published datasets

Preprocessed expression count data were obtained from Karsten Bach (21) and analyzed using scripts provided by Bach et al., modified to compare the C12 vs C14 clusters and C13 vs C14 clusters using edgeR 3.22.5 in R 3.5.1 (22). An R script to generate the differential expression results between these clusters is available at: (https://gist.github.com/adamewing/2819d7e5072aa35632bba7f51236446b). Violin and volcano plots were generated using the seaborn package for python (23); zero counts were removed. Scripts are available at: (https://gist.github.com/adamewing/931cc44d717959073fa5b09078e7e4b3) and (https://gist.github.com/adamewing/90f1f57985a2033f292debb2e2e5b25f) respectively. Gene Set Enrichment Analysis (GSEA) (24) was carried out using genes ranked by fold change.

Supplementary References

1. Sherman ME, et al. (2012) The Susan G. Komen for the Cure Tissue Bank at the IU Simon Cancer Center: A unique resource for defining the “molecular histology” of the breast. *Cancer Prev Res* 5(4):528–535.
2. Davis FM, et al. (2016) Single-cell lineage tracing in the mammary gland reveals stochastic clonal dispersion of stem/progenitor cell progeny. *Nat Commun* 7:13053.
3. Lloyd-Lewis B, et al. (2016) Imaging the mammary gland and mammary tumours in 3D: Optical tissue clearing and immunofluorescence methods. *Breast Cancer Res* 18(1).
4. Susaki EA, et al. (2014) Whole-brain imaging with single-cell resolution using chemical cocktails and computational analysis. *Cell* 157(3):726–39.
5. Ke M-T, Fujimoto S, Imai T (2013) SeeDB: a simple and morphology-preserving optical clearing agent for neuronal circuit reconstruction. *Nat Neurosci* 16(8):1154–61.
6. Lloyd-Lewis B, Davis FM, Harris OB, Hitchcock JR, Watson CJ (2018) Neutral lineage tracing of proliferative embryonic and adultmammary stem/progenitor cells. *Development* 145(14):164079.
7. Linkert M, et al. (2010) Metadata matters: access to image data in the real world. *J Cell Biol* 189(5):777–782.
8. Schindelin J, et al. (2012) Fiji: an open source platform for biological image analysis. *Nat Methods* 9(7):676–682.
9. Boulanger J, et al. (2010) Patch-based nonlocal functional for denoising fluorescence microscopy image sequences. *IEEE Trans Med Imaging*. doi:10.1109/TMI.2009.2033991.
10. Prater M, Shehata M, Watson CJ, Stingl J (2013) Enzymatic dissociation, flow

cytometric analysis, and culture of normal mouse mammary tissue. *Methods MolBiol* 946:395–409.

11. Jardé T, et al. (2016) Wnt and Neuregulin1/ErbB signalling extends 3D culture of hormone responsive mammary organoids. *Nat Commun* 7:13207.
12. Davis FM, et al. (2015) Essential role of Orai1 store-operated calcium channels in lactation. *Proc Natl Acad Sci* 112(18):5827–5832.
13. Masedunskas A, Chena Y, Stussman R, Weigert R, Mather IH (2017) Kinetics of milk lipid droplet transport, growth, and secretion revealed by intravital imaging: Lipid droplet release is intermittently stimulated by oxytocin. *Mol Biol Cell* 28:935–946.
14. Dawson CA, et al. (2020) Tissue-resident ductal macrophages survey the mammary epithelium and faciliate tissue remodelling. *Nat Cell Biol*.
15. Stewart TA, et al. (2019) Mammary mechanobiology: mechanically-activated ion channels in lactation and involution. *bioRxiv*:649038.
16. Avants BB, Epstein C, Grossman M, Gee JC (2008) Symmetric diffeomorphic image registration with cross-correlation: evaluating automated labeling of elderly and neurodegenerative brain. *Med Image Anal* 12(1):26–41.
17. Avants BB, et al. (2011) A reproducible evaluation of ANTs similarity metric performance in brain image registration. *Neuroimage* 54(3):2033–44.
18. Jia H, Rochefort NL, Chen X, Konnerth A (2011) In vivo two-photon imaging of sensory-evoked dendritic calcium signals in cortical neurons. *Nat Protoc* 6:28–35.
19. Giovannucci A, et al. (2019) CaImAn an open source tool for scalable calcium imaging data analysis. *Elife* 8:e38173.
20. Mackevicius EL, et al. (2019) Unsupervised discovery of temporal sequences in high-dimensional datasets, with applications to neuroscience. *Elife* 8:e38471.
21. Bach K, et al. (2017) Differentiation dynamics of mammary epithelial cells revealed by single-cell RNA sequencing. *Nat Commun* 8:2128.
22. Robinson MD, McCarthy DJ, Smyth GK (2009) edgeR: A Bioconductor package for differential expression analysis of digital gene expression data. *Bioinformatics* 26(1):139–40.
23. Waskom M, et al. (2018) mwaskom/seaborn: v0.9.0 (July 2018). doi:10.5281/ZENODO.1313201.
24. Subramanian A, et al. (2005) Gene set enrichment analysis: A knowledge-based approach for interpreting genome-wide expression profiles. *Proc Natl Acad Sci* 102(43):15545–15550.